Journal of Magnetic Resonance **150,** 167–174 (2001)
doi:10.1006/jmre.2001.2325, available online at http://www.idealibrary.com on IDEAL®

Probing Proteins in Solution by ^{129}Xe NMR Spectroscopy

Emanuela Locci, Yves Dehouck,* Mariano Casu, Giuseppe Saba, Adolfo Lai, Michel Luhmer,* Jacques Reisse,* and Kristin Bartik*,[1]

*Dipartimento di Scienze Chimiche, Università di Cagliari, 09042 Monserrato (CA), Italy; and *Laboratoire de Chimie Organique E.P., Université Libre de Bruxelles, 1050 Brussels, Belgium*

Received October 16, 2000; revised January 31, 2001; published online May 10, 2001

The interaction of xenon with different proteins in aqueous solution is investigated by ^{129}Xe NMR spectroscopy. Chemical shifts are measured in horse metmyoglobin, hen egg white lysozyme, and horse cytochrome *c* solutions as a function of xenon concentration. In these systems, xenon is in fast exchange between all possible environments. The results suggest that nonspecific interactions exist between xenon and the protein exteriors and the data are analyzed in term of parameters which characterize the protein surfaces. The experimental data for horse metmyoglobin are interpreted using a model in which xenon forms a 1 : 1 complex with the protein and the chemical shift of the complexed xenon is reported (Locci *et al.*, Keystone Symposia "Frontiers of NMR in Molecular Biology VI," Jan. 9–15, 1999, Breckenridge, CO, Abstract E216, p. 53; Locci *et al.*, XeMAT 2000 "Optical Polarization and Xenon NMR of Materials," June 28–30, 2000, Sestri Levante, Italy, p. 46).

Key Words: **xenon; NMR; protein cavities; protein surfaces.**

INTRODUCTION

Xenon is a highly polarizable, hydrophobic, and chemically inert atom, which has a van der Waals radius of ≈2 Å. Two xenon isotopes are easily accessible to NMR spectroscopy: ^{129}Xe ($I = 1/2$, natural abundance of 26.4%) and ^{131}Xe ($I = 3/2$, natural abundance of 21.2%) (*3*).

In our paper of 1986 (*4*), we already pointed out the potential importance of monoatomic xenon NMR for the study of intermolecular interactions in solution. At that time, xenon NMR was extensively used to obtain valuable information about the internal structure of zeolites and clathrates in the solid state and to study intermolecular interactions involving xenon in the gas phase (see the reviews by Dybowski *et al.* (*5*) and by Raftery and Chmelka (*6*)). Even though the number of solution studies was scarce, it was already clear that xenon was potentially an efficient spin-spy for the liquid phase. Xenon can be regarded as a spin-spy because of the extreme sensitivity of its chemical shift to the local environment and of its relaxation rates to the dynamics of the surroundings. Chemical shift studies are in general performed with the ^{129}Xe isotope. Relaxation studies are more frequently performed using the quadrupolar ^{131}Xe isotope.

We have been involved in xenon NMR studies for more than 15 years. Our work has been devoted to the study of xenon dissolved in solvents (*7–14*) and in dilute solutions of host molecules which can complex xenon (*15–21*). These studies concerned chemical shift and relaxation rate measurements and also computer experiments based on molecular dynamics and equilibrium thermodynamics. The present work is an example of a study which comprises both ^{129}Xe chemical shift measurements and computer experiments using a thermodynamic model previously developed in our laboratory (*16*). The aim of this work is to probe the hydrophobic cavities and surfaces of proteins.

Cavities exist in proteins and several molecular modeling studies undertaken to characterize some of their general properties have been reported in the literature (*22–25*). There is a great interest in the study of protein cavities because the precise role of cavities in the interior of most proteins remains unknown. The use of xenon to study these cavities is certainly not new. In the 1960s, Schoenborn *et al.* showed by X-ray crystallography that xenon can be absorbed within well-defined hydrophobic cavities in myoglobin (*26–28*) and hemoglobin (*29*). They showed that sperm whale metmyoglobin under 2.5 atm of xenon binds xenon in its proximal cavity (*26*). This site is also almost fully occupied in sperm whale deoxymyoglobin (*27*) and alkaline metmyoglobin (pH 9.1) (*28*). A second lower occupancy binding site is also observed in the alkaline metmyoglobin. More recently, four binding sites, with occupancies ranging between 0.4 and 0.95, were observed in sperm whale metmyoglobin equilibrated with 7 atm of xenon and the highest occupancy site is the proximal cavity (*30*). Very little perturbation of the surrounding molecular structure is observed. Equilibrium constants for xenon horse myoglobin, metmyoglobin, and cyanometmyoglobin complexes were derived from xenon absorption measurements (*31*). For metmyoglobin, it was concluded that two xenon binding sites exist and that the equilibrium constants range, depending on temperature, between 85 and 200 M^{-1} and between 1 and 10 M^{-1}.

In 1982, Tilton and Kuntz were the first to use ^{129}Xe NMR to study the complexation of xenon by sperm whale myoglobin and hemoglobin (*32*). From a study of the variation of the ^{129}Xe

[1] To whom correspondence should be addressed at Laboratoire de Chimie Organique E.P. (CP165/64), Université Libre de Bruxelles, 50 Avenue F.D. Roosevelt, 1050 Bruxelles, Belgium. Fax: 32-2-650 3606. E-mail: kbartik@ulb.ac.be.

1090-7807/01 $35.00

chemical shift and linewidth with temperature (−50 to 10°C using a cryosolvent) under 1 atm of xenon, the authors concluded that a single xenon binding site exists in methemoglobin while two distinct xenon binding sites exist in metmyoglobin. However, a single binding constant of 77 M^{-1} is estimated for metmyoglobin and it is interpreted as the average binding constant for the two binding sites. An association rate constant of 1.8 10^7 $M^{-1}\,s^{-1}$ is calculated, but the value of 190 M^{-1} reported for the binding constant in horse metmyoglobin (*31*) was used to arrive at this result. They also report the variation, at atmospheric pressure and ambient temperature, of the chemical shift of xenon with metmyoglobin concentration. They conclude from these measurements that the chemical shift of the bound xenon is upfield of the chemical shift of xenon in water. They demonstrated clearly that xenon NMR could become a powerful tool to study the protein structure and, more precisely, internal cavities in proteins.

After Tilton and Kuntz reported their results, various research groups, including the Tilton group, performed complementary studies on xenon–protein complexes using X-ray crystallography (*30, 33–35*) and molecular dynamics (*36, 37*). Computational studies were performed on the xenon–metmyoglobin system to investigate the binding energies of xenon in the cavities and the effect of protein motions on xenon trajectories in the protein (*37*). The empirical energy calculations indicate a favorable enthalpic contribution to xenon binding, the largest contribution coming from van der Waals interactions. These calculated enthalpies help explain the different xenon occupancies observed experimentally at 7 atm of xenon. Molecular dynamics simulations show that transient cavities, with lifetimes of the order of 10 to 20 ps, play a crucial role in the movement of the xenon atoms in the protein and that the binding sites are inaccessible to the ligand without cooperative protein motions to allow passage (*36*).

We had to wait until 1999 to find another paper in the literature which reports the use of xenon NMR to explore hydrophobic sites in proteins (*38*). In this study, the work of Tilton and Kuntz is reproduced and the variation of the xenon chemical shift and linewidth with temperature in horse metmyoglobin solutions was found to be in good agreement with the original work. Hyperpolarized xenon was also used to study the interaction of xenon with different lyophilized proteins (horse metmyoglobin, horse methemoglobin, hen egg white lysozyme, and soybean lipoxygenase) in the solid state at low temperatures. The authors concluded from an analysis of the resonance lineshapes that xenon is undergoing exchange between the gas phase and several unresolved sites associated with the protein surface or with cavities. A second paper published in 1999 reports the use of hyperpolarized xenon to measure the apparent ^{129}Xe spin–lattice relaxation rate of xenon dissolved in horse apomyoglobin and metmyoglobin solutions (*39*). These relaxation rates were found to be significantly larger than the ^{129}Xe relaxation rate in D_2O. According to the authors, this increase is a result of the efficient relaxation pathways available to xenon bound in the proteins.

Considering that neither the paper of Tilton and Kuntz nor these last two papers used a thermodynamic model to obtain quantitative data on xenon–protein interactions, we decided to adapt the treatment we developed for the α-cyclodextrin–xenon system and to apply it to study xenon–protein interactions. Our results were presented as communications in 1999 and 2000 at international meetings (*1, 2*). When our manuscript was near completion we learnt of the very recent publication of a paper by Rubin *et al.* devoted to a similar problem (*40*). In this paper they used a variant of the thermodynamic "three-site" model which we introduced in the literature in 1995 (*16*) but they performed their experiments with hyperpolarized xenon while we used thermally polarized xenon. They worked with horse metmyoglobin while we worked with three different proteins, horse metmyoglobin, hen egg white lysozyme, and horse cytochrome *c*, at different concentrations. The interest in comparing different proteins lies in the fact that the "three-site" models takes three different xenon environments into account: xenon in bulk (identical to xenon in pure water), xenon in hydrophobic cavities, and, very importantly, xenon at the protein surface. A innovative way to probe this last environment consists of studying xenon chemical shifts in the presence of proteins which do not have specific xenon binding sites. We have also performed computer experiments in order to test the parametric sensitivity of our thermodynamic model. These are the major originalities of our work with respect to the work previously published.

MATERIALS AND METHODS

Salt-free crystallized and lyophilized horse skeletal muscle myoglobin (MMb), hen egg white lysozyme (HEWL), and horse heart cytochrome *c* (Cyt-c) were purchased from Sigma and used without further purification. Xenon gas at natural isotope abundance (purity of 99.99%) was purchased from SIAD (Italy) and from Air Liquide (Belgium). Wilmad high-pressure NMR tubes (OD 10 mm and ID 7.1 mm) were used for all measurements.

Protein solutions were freshly prepared at room temperature by dissolving the protein in H_2O/D_2O (80/20). MMb samples were filtered through a membrane (0.45 μm PP). The exact protein concentrations were determined spectrophotometrically at $\lambda_{max} = 280$ nm ($\varepsilon_{MMb} = 31{,}000\ M^{-1}\,cm^{-1}$ (*41*) and $\varepsilon_{HEWL} = 36{,}975\ M^{-1}\,cm^{-1}$ (*42*)), and at $\lambda_{max} = 409$ nm ($\varepsilon_{Cyt-c} = 91{,}970\ M^{-1}\,cm^{-1}$, CRC Handbook of Biochemistry). A 2 mM cyanometmyoglobin solution was prepared by adding 10 equivalents of NaCN to a 2 mM MMb solution.

Samples of known volume (≈2 ml) were placed in the NMR tube of known volume (≈8 ml). Samples were then degassed on a vacuum line without freezing the solution to avoid protein denaturation. Up to 10 atm of xenon gas was pressurized into the samples at room temperature. The samples were left to equilibrate for 1 h before the spectra were acquired. The total amount of xenon added to the NMR tube was known precisely from the difference between the weight of the sample after xenon addition and the weight of the degassed sample.

The UV-visible spectra of aqueous MMb samples, in the absence and in the presence of xenon, were characteristic of a high-spin hemoprotein with absorption maxima at 505 and 640 nm (*43*). The ^{1}H NMR spectra showed the typical signals characteristic of a high-spin hemoprotein in the downfield spectral region (20–100 ppm) (*44*).

Titrations of MMb with HgI_3^- were done by dilution of the protein into solutions containing different concentrations of $KHgI_3$ (HgI_2 with an excess of KI).

^{129}Xe NMR spectra in horse myoglobin solutions were recorded on a Varian VXR-300 spectrometer at a resonance frequency of 82.97 MHz. The chemical shift measurements were carried out using a 21-μs pulse (90°), a 0.5-s repetition time, and a spectral width of 20,000 Hz. ^{129}Xe NMR spectra in HEWL and Cyt-c solutions were recorded on a Bruker AMX360 spectrometer at a resonance frequency of 99.64 MHz. The chemical shift measurements were carried out using a 10-μs pulse (90°), a 5-s repetition time, and a spectral width of 8062 Hz. All spectra were referenced to the chemical shift of pure xenon gas extrapolated to zero pressure. To obtain this reference, spectra were recorded for different amounts of pure xenon gas pressurized into the Wilmad high-pressure NMR tube. The number of scans recorded varied from spectrum to spectrum so as to obtain a good signal-to-noise ratio. It was very difficult to obtain experimental data at very low xenon concentrations (experimental time >30 h). The temperature was controlled at 25.0 ± 0.1°C.

For the computer simulations two sets of 20 data points were chosen in the following manner.

In the first set, the data points were distributed in the whole xenon concentration range: six data points were equally distributed in the range $0 < (n\mathrm{Xe}/V_\mathrm{l}) \leq 0.13$ M and 14 additional points were distributed every 0.1 M in the range $0.2\ \mathrm{M} \leq (n\mathrm{Xe}/V_\mathrm{l}) < 1.5$ M ($n\mathrm{Xe}/V_\mathrm{l}$ = total number of moles of xenon in the NMR tube divided by the volume of solution).

In the second set, the data points were distributed in the experimentally accessible xenon concentration range. The first five points from the first set were eliminated and five additional points were added between $0.13\ \mathrm{M} < (n\mathrm{Xe}/V_\mathrm{l}) < 0.6$ M.

Surface and volume calculations and the determination of the residues constituting the protein external and cavities surfaces were performed using the molecular modeling program SURVOL (*45*). The probe size used was 2 Å.

RESULTS AND DISCUSSION

^{129}Xe NMR spectra were recorded at 25°C for horse metmyoglobin solutions containing increasing amounts of xenon (the pressure ranged between 0 and 10 atm). A single resonance line is observed in all spectra, indicating that the xenon is in fast exchange between all available environments. Figure 1 represents the variation of the observed ^{129}Xe NMR chemical shift as a function of the total number of moles of xenon in the NMR tube divided by the volume of solution ($n\mathrm{Xe}/V_\mathrm{l}$); the three curves correspond to three different protein concentrations. The xenon

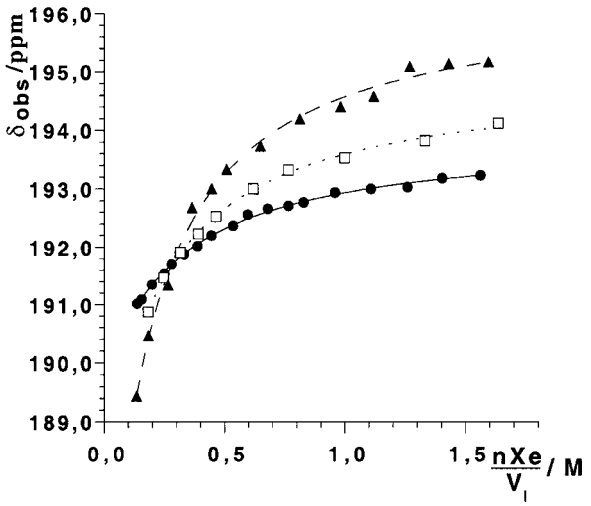

FIG. 1. Variation of the observed ^{129}Xe chemical shift as a function of the total number of moles of xenon in the NMR tube divided by the volume of solution ($n\mathrm{Xe}/V_\mathrm{l}$) in 0.8 mM (●), 1.2 mM (□), and 2.1 mM (▲) solutions of MMb. The lines correspond to the results of the best fitting obtained when K, δ_{in}, and δ_{out} are taken as independent parameters (results shown in columns 2, 3, and 4 of Table 1).

linewidths are large in all spectra (between 500 and 50 Hz). They decrease when the amount of xenon added to the NMR tube increases and when the protein concentration decreases. At low xenon concentrations an upfield shift is observed for the Xe resonance relative to the Xe resonance in the solvent (80% H_2O/20% D_2O; $\delta = 192.3$ ppm). As the xenon concentration increases, the xenon resonance shifts downfield.

As mentioned in the Introduction, X-ray data have shown that four complexation sites exist for xenon in sperm whale MMb and that one of these sites is the proximal cavity on one side of the heme group. On average, even at 7 atm, only two of the four xenon binding sites are occupied at any time, the proximal site being by far the most populated (*30*). In horse myoglobin solutions, the xenon resonance line is influenced by the oxidation and spin state of the iron in the heme group. We observed that the xenon linewidth in 2 mM cyanometmyoglobin (Fe^{3+}, $S = 1/2$) solutions ranges between 175 and 80 Hz while in 2 mM metmyoglobin solutions (Fe^{3+}, $S = 5/2$) it ranges between 400 and 150 Hz. This suggests that xenon is also complexed in the proximal cavity of MMb.

A large difference is reported between the two equilibrium constants characterizing the binding of xenon to horse MMb (146 and 7 M^{-1} at 25°C) (*31*). We therefore believe that, at first approximation, the chemical shift variation observed with xenon pressure in horse MMb solutions can be analyzed using a model in which xenon forms a 1:1 complex with the protein and exchanges rapidly between the proximal binding site ($\mathrm{Xe}_{\mathrm{in}}$) and all other environments ($\mathrm{Xe}_{\mathrm{out}}$):

$$\mathrm{MMb} + \mathrm{Xe}_{\mathrm{out}} \rightleftharpoons \mathrm{Xe}_{\mathrm{in}} \quad K = \frac{[\mathrm{Xe}]_{\mathrm{in}}}{[\mathrm{Xe}]_{\mathrm{out}}[\mathrm{MMb}]}. \qquad [1]$$

The observed chemical shift of ^{129}Xe can therefore be expressed in the following manner,

$$\delta_{obs} = \delta_{out} + (\delta_{in} - \delta_{out})\frac{[Xe]_{in}}{[Xe]_l}, \quad [2]$$

where δ_{in} = the chemical shift of complexed xenon, i.e., xenon trapped in the proximal cavity, δ_{out} = the chemical shift of uncomplexed xenon which corresponds to the average chemical shift for all the other possible environments for xenon, $[Xe]_{in} = nXe_{in}/V_l$ = the concentration of complexed xenon, and $[Xe]_l = (nXe_{in} + nXe_{out})/V_l$ = the total concentration of xenon in solution.

If the assumptions are made that xenon is an ideal gas, that Henry's law holds, and that xenon does not have an increased affinity for the protein surface, $[Xe]_{out}$ corresponds to the concentration of xenon in the pure solvent and can be given by the equation

$$[Xe]_{out} = \frac{nXe_{out}}{V_l} = H\frac{nXe_g}{V_g} \quad \text{with } H = RT[Xe]^o, \quad [3]$$

where $[Xe]^o$ (M atm^{-1}) corresponds to the variation with pressure of the solubility of xenon in water at 25°C, V_l and V_g are the volumes of liquid and gas phases in the NMR tube, and nXe_g is the number of moles of xenon in the gas phase. Using the mass balance equation for xenon ($nXe = nXe_g + nXe_{out} + nXe_{in}$), the above equation leads to

$$[Xe]_{out} = g\left(\frac{nXe}{V_l} - [Xe]_{in}\right) \quad \text{with } g = \frac{\frac{V_l}{V_g}H}{1 + \frac{V_l}{V_g}H}. \quad [4]$$

Using Eqs. [1] and [4] it is possible to write the ratio $[Xe]_{in}/[Xe]_l$ in terms of K and of the known quantities nXe, V_l/V_g, and H. The variation of δ_{obs} with nXe/V_l will therefore be a function of three parameters: δ_{in}, δ_{out}, and K.

Fitting the model to the experimental data gives the values of δ_{in}, δ_{out}, and K listed in Table 1. The values of K and δ_{in} should be identical within experimental error for the three protein concentrations. To understand why this is not the case, we carried out the following computer simulations. Using our model and chosen values for the three parameters ($K = 200$ M^{-1}, $\delta_{in} = 152$ ppm, and $\delta_{out} = 193.5$ ppm), we calculated the xenon chemical shifts for a protein concentration of 0.7 mM. Two sets of 20 points were selected from this theoretical curve. In the first set, the points were distributed over the whole xenon concentration range ($0 < (nXe/V_l) \leq 1.5$ M) and in the second set the points were distributed in the experimentally accessible xenon concentration range (0.13 M $\leq (nXe/V_l) \leq 1.5$ M). A randomly generated error of less than ± 0.1 ppm was added to these points and the new chemical shift values were treated as experimental data points and submitted to a best fitting procedure using our model. This procedure was repeated 180 times for both sets of points. The distribution of the values obtained for δ_{in}, δ_{out}, and K are presented in Fig. 2. Analysis of these distributions clearly show that if we wish to obtain the three parameters with good accuracy and precision it is necessary to have data points located in the low xenon concentration range which corresponds to xenon overpressures of less than 0.5 atm. Unfortunately, it is very difficult to obtain xenon NMR spectra from which it is possible to extract reliable data for this concentration range. If we had only studied one protein concentration we would not have become aware of this problem.

TABLE 1

Equilibrium Constant (K) and ^{129}Xe Chemical Shifts (δ_{in}, δ_{out}) Obtained from Fitting the Three Parameter Model to the Experimental Data

[MMb] (mM)	K (M^{-1})	δ_{in} (ppm)	δ_{out} (ppm)	δ^*_{in} (ppm)	δ^*_{out} (ppm)
0.8	115 ± 10	140 ± 4	193.9 ± 0.1	148.5 ± 0.6	193.8 ± 0.1
1.2	185 ± 28	156 ± 3	194.9 ± 0.1	150.0 ± 0.7	195.1 ± 0.1
2.1	323 ± 91	165 ± 3	196.3 ± 0.2	151 ± 1	196.9 ± 0.1

Note. The errors are fitting errors (*47*). ^{129}Xe chemical shifts (δ^*_{in}, δ^*_{out}) were obtained from fitting the same model to the experimental data with K fixed at 146 M^{-1}.

By fixing K to the value reported in the literature for the xenon–horse MMb system in aqueous solution (146 M^{-1} at 298 K) (*31*), we were able to derive the two other parameters, δ_{in} and δ_{out} (results also reported in Table 1). δ_{in} is now independent of the protein concentration (the differences are within experimental error). The value obtained is very close to the value that Tilton and Kuntz report as being the chemical shift of xenon in the "protein site" in sperm whale MMb. Indeed, they report a value of −43 ppm from the Xe resonance in 70% H_2O/30% D_2O (at atmospheric pressure), whereas we obtain a value of −42.1 ppm from the Xe resonance in 80% H_2O/20% D_2O (at 10 atm). We must, however, for several reasons, be extremely cautious in the quantitative comparison of these values. First, our value of δ_{in} is sensitive to the value chosen for K to fit the experimental data. A change in K of 10 M^{-1} leads to a change in δ_{in} of ≈2 ppm. Second, Tilton and Kuntz obtain their value by extrapolating the chemical shift of xenon at atmospheric pressure in protein solutions to infinite protein concentration even though they do not have many data points in the high protein concentration range (highest concentration is around 20 mM). Last, but not least, it is possible that the difference in the amino acid sequences of horse and sperm whale MMb could influence the value of δ_{in}, even if none of the differences concern residues which are reported to be close to the xenon atom in the crystal structure of the xenon–sperm whale MMb complex (*26*).

As mentioned in the Introduction, Rubin *et al.* used a variant of our "three site" model to analyze the variation of xenon chemical shift in a 5 mM solution of MMb (*40*). Not surprisingly, they found that in order to fit their data uniquely they had to fix the value of K. Their experiments were run at 298 K but they chose a

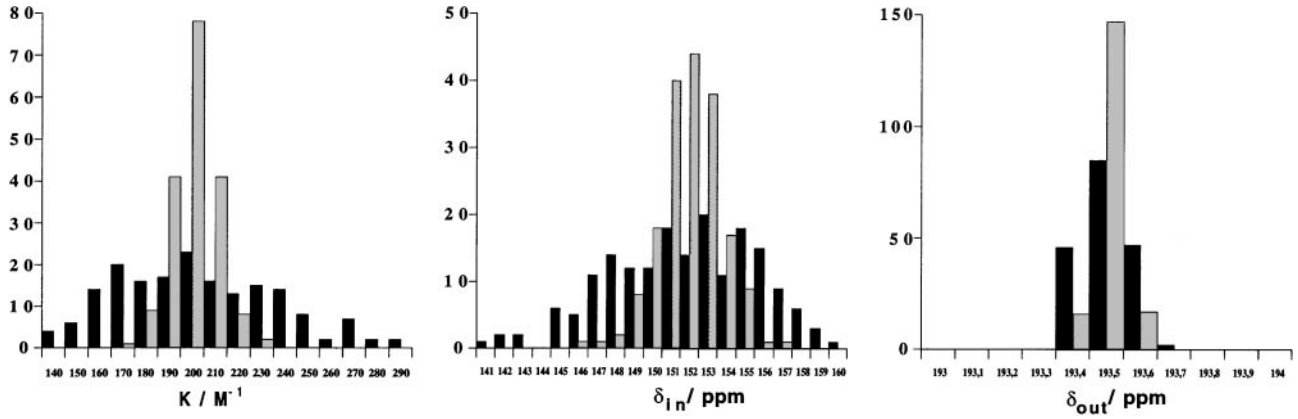

FIG. 2. Distribution of the values for K, δ_{in}, and δ_{out} obtained via the computer simulations. The dark bars correspond to the results obtained using the narrower range of $n\mathrm{Xe}/V_l$ values and the lighter bars correspond to the results obtained using the larger range of $n\mathrm{Xe}/V_l$ values.

value for K of 190 M^{-1}, which is the value reported for the equilibrium constant at 293 K (*31*). They report a value for δ_{in} which is -20 ppm from the Xe resonance in 80% H_2O/20% D_2O. This value is significantly smaller than ours but they have very few data points, especially in the low xenon concentration range (no data point for a xenon overpressure of less than 1 atm).

δ_{out} is proportional to the protein concentration (Fig. 3). The dependence of δ_{out} on protein concentration shows that xenon interacts nonspecifically with the protein surface and this chemical shift is the average value between the chemical shifts of xenon in the pure solvent and xenon in contact with the protein surface. Since the fraction of xenon in contact with the protein surface is proportional to the protein concentration, the observed dependence on protein concentration is to be expected.

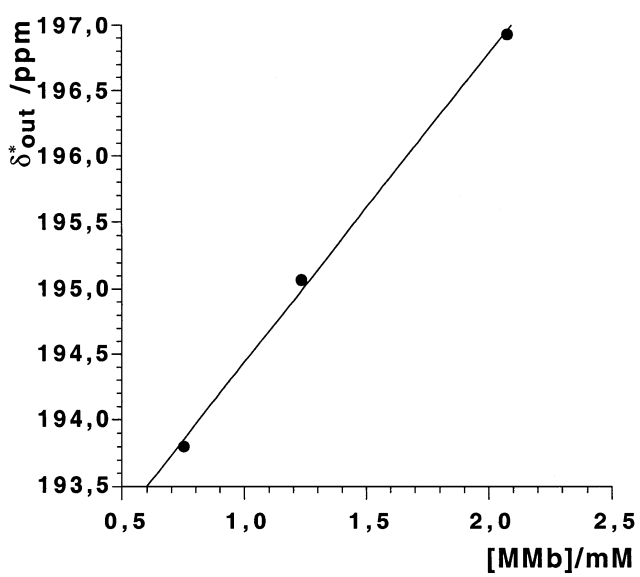

FIG. 3. Chemical shift of uncomplexed xenon (δ^*_{out}) as a function of MMb concentration.

It is known from X-ray data that HgI_3^- binds in the proximal cavity of sperm whale MMb (*46*). Tilton and Kuntz report competitive binding between xenon and HgI_3^- for the protein (*32*). They observe a limiting xenon chemical shift when the xenon–sperm whale MMb system is titrated with HgI_3^- and the xenon linewidth decreases from 200 to 20–30 Hz. We titrated our system with HgI_3^- with the hope of blocking the xenon complexation site. If this site is not accessible to xenon, the observed xenon chemical shift will be a function of the nonspecific interactions between xenon and the protein exterior or, in other words, a direct measure of δ_{out}. We observed that horse MMb does not complex HgI_3^- in its proximal cavity. Indeed, the xenon linewidths do not decrease when the xenon–horse MMb system is titrated with HgI_3^- (up to a 10 : 1 ratio of HgI_3^- to protein), indicating that the proximal cavity is still accessible to xenon. It is clear that the availability of this site is very sensitive to the precise conformation of the protein. Horse and sperm whale myoglobin differ by 19 amino acids and the changes in the atomic distribution seem to have a marked effect on the binding properties of the protein.

We thought that it might be possible to quantify the nonspecific interactions of xenon with the protein surface, and thereby obtain a value for δ_{out}, by studying the interaction of xenon with proteins which do not have a specific xenon binding site. This approach is similar to the one that we used previously when studying the complexation of xenon by α-cyclodextrin in solution (*16*). In that study, we used maltohexaose in order to estimate the contribution of the nonspecific interaction of xenon on the observed chemical shift. The approach used by Rubin *et al.* (*40*) was to study denatured metmyoglobin in solution. Since xenon is extremely sensitive to its environment, the measured chemical shift is certainly influenced by the buried residues which become accessible when the protein is denatured and also by the presence of 6 M urea. We measured the xenon chemical shift in solutions of hen egg white lysozyme and horse cytochrome *c*. We chose these two proteins because they have roughly the same number of residues as MMb and also similar

dimensions (HEWL: 129 residues, accessible surface measured by SURVOL = 6500 Å^2; Cyt-c: 104 residues, accessible surface = 6000 Å^2; MMb: 153 residues, accessible surface = 7700 Å^2). X-ray data have shown that HEWL can complex xenon in an internal cavity (*35*). However, the occupancy factor of this cavity is relatively low (0.28) and we believe that for our experimental conditions (below 10 atm) this cavity will not be significantly occupied. To our knowledge no X-ray studies of the interaction of xenon and cytochrome *c* have been reported. Analysis of X-ray structures of cytochrome *c* (PDB code: 1HRC), using the SURVOL molecular modeling software, suggest that no cavity large enough to accommodate a xenon atom exists in this protein and that none can be created with small structure perturbations.

^{129}Xe NMR spectra were recorded at 25°C for solutions of both proteins containing increasing amounts of xenon (the pressure ranged between 1 and 10 atm). A single sharp resonance line (linewidth less than 20 Hz in HEWL solutions and less than 10 Hz in Cyt-c solutions) is observed in all of the spectra. Since we suppose that there are no specific xenon complexation sites which are significantly occupied in these proteins, the chemical shift of this resonance line corresponds to δ_{out}. If we assume, like we did for MMb, that xenon is an ideal gas, that Henry's law holds, and that xenon does not have an increased affinity for the protein surface and if we consider that the volume occupied by the protein (V_p) is small compared to the solution volume (we estimate V_p to be ≈3% of V_l for the highest protein concentration), it is possible to calculate, for these systems, the xenon concentration in solution, $[Xe]_l$. Indeed, this quantity can be calculated from the total number of moles of xenon added to the sealed NMR tube and the exact volumes of the liquid and the gas phases. Figures 4a and 4b represent the variation of the observed ^{129}Xe NMR chemical shift for different HEWL and Cyt-c concentrations as a function of xenon concentration in solution. The variation of the ^{129}Xe NMR chemical shift in the solvent (80% H_2O/20% D_2O) is also shown in Fig. 4a.

The fact that the xenon chemical shift in HEWL and Cyt-c solutions is a linear function of $[Xe]_l$ shows us that our MMb data should have been analyzed with an additional parameter which characterizes the linear dependence of δ_{out} with $[Xe]_l$. However, we see that the variation δ_{out} in Figs. 4a and 4b is less than 0.3 ppm, which is of the same order of magnitude as the error attached to the determination of δ_{out} in the horse MMb system. We can, however, analyze the HEWL and Cyt-c data to obtain more information on the chemical shift of xenon at the protein surface. Indeed, as mentioned previously, δ_{out} is an average value between the chemical shift of xenon in the pure solvent (δ_b) and the chemical shift of xenon in contact with the protein surface (δ_s). The protein surface is constituted of different residues and we consider δ_s an averaged value for xenon at the surface. The chemical shift can therefore be expressed in the as

$$\delta_{out} = \frac{n\mathrm{Xe}_s}{n\mathrm{Xe}_l}(\delta_s - \delta_b) + \delta_b, \qquad [5]$$

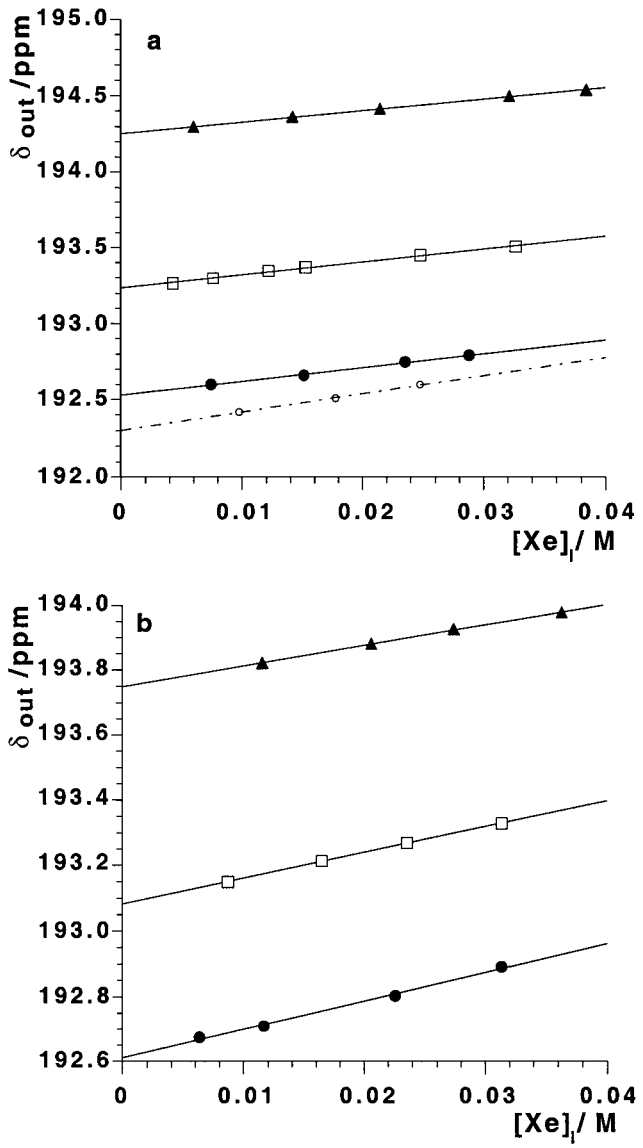

FIG. 4. (a) Variation of ^{129}Xe chemical shift as a function of $[Xe]_l$ in the pure solvent, 80% H_2O/20% D_2O (○), and in 0.9 mM (●), 1.7 mM (□), and 4.3 mM (▲) solutions of HEWL. (b) Variation of ^{129}Xe chemical shift as a function of $[Xe]_l$ in 1.0 mM (●), 2.4 mM (□), and 4.8 mM (▲) solutions of Cyt-c.

where δ_s = the chemical shift of xenon at the protein surface, δ_b = the chemical shift of xenon in the bulk which corresponds to the chemical shift of xenon in the solvent, $n\mathrm{Xe}_s/n\mathrm{Xe}_l$ = the molar fraction of xenon at the protein surface, and $n\mathrm{Xe}_l = n\mathrm{Xe}_s + n\mathrm{Xe}_b$ = the total number of moles of xenon in solution.

It is not obvious why the chemical shift of xenon observed in $H_2O/D_2O(\delta_b)$ varies with xenon concentration. It is possible that the formation of clathrates of xenon, which is hydrophobic, plays a role. If we express the variation of δ_b as a function of $[Xe]_l$ as $A_0 + B_0[Xe]_l$, for a given protein concentration Eq. [5]

becomes

$$\delta_{out} = A + B[Xe]_l \quad \text{where} \quad A = A_0 + \frac{nXe_s}{nXe_l}(\delta_s - A_0) \qquad B = B_0\left(1 - \frac{nXe_s}{nXe_l}\right). \qquad [6]$$

For a given protein, we expect δ_s to be independent of xenon concentration and the molar fraction of xenon at the protein surface (nXe_s/nXe_l) to be proportional to the protein concentration. Analysis of Eq. [6] shows that the slope (B) and the intercept (A) of the variation of δ_{out} with $[Xe]_l$ should be linear with the protein concentration. As shown in Figs. 5a and 5b, this is indeed the case. From the data represented in these figures, it is possible to obtain a value for the δ_s of both proteins: $\delta_s = 202 \pm 1$ ppm for HEWL and $\delta_s = 197 \pm 1$ ppm for Cyt-c. These results show that xenon is sensitive enough to differentiate the two protein surfaces. We characterized the residues at the protein surfaces in terms of their hydrophobicity, charge, and polarity. The biggest differences between HEWL and Cyt-c surfaces concern the proportion of charged and polar residues. Whereas in Cyt-c the percentage of charged residues is higher than in the HEWL surface (55% vs 40%), it is the contrary for the polar residues (20% vs 35%). With the data that we have it is, however, not obvious to establish a correlation between the value of δ_s and the nature of the surface residues.

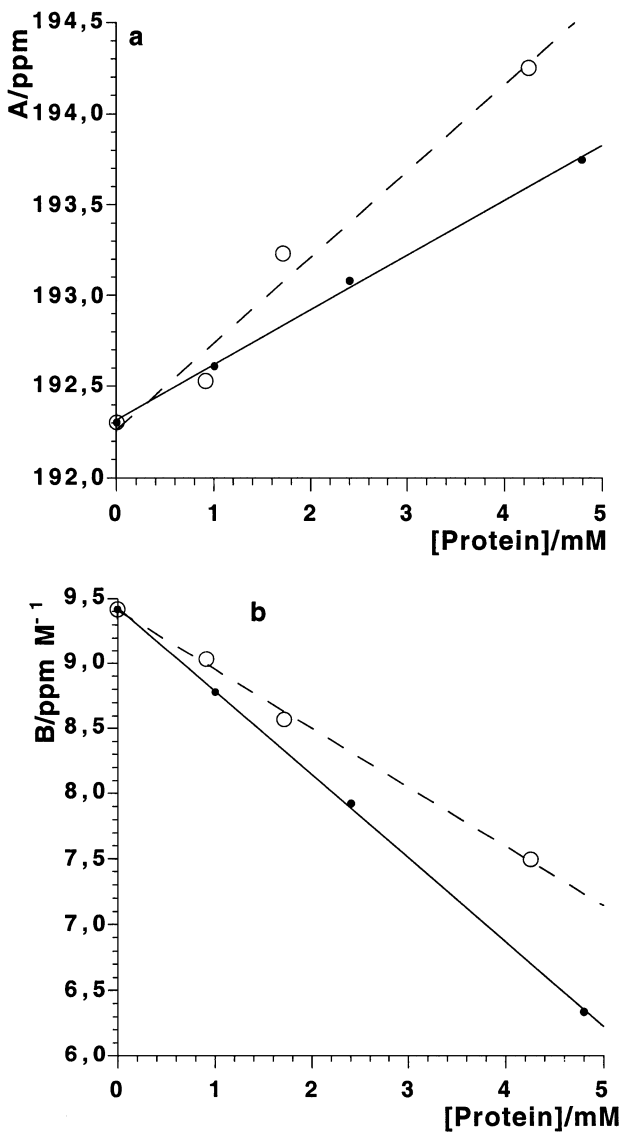

FIG. 5. (a) Intercept, A, and (b) slope, B, of the variation of δ_{out} vs $[Xe]_l$ as a function of the concentration of HEWL (○) and Cyt-c (●).

CONCLUSIONS

Our work was essentially devoted to a methodological study of the possibilities that xenon NMR offers for the structural study of proteins. It clearly shows that the extreme sensitivity of xenon chemical shift to its environment offers many advantages. Indeed, xenon acting as a spin-spy is clearly able to detect very subtle differences between various protein environments. However, the sensitivity is so high that experimentally significant differences are difficult to explain. This is particularly true for the protein surface effects. To further the interpretation it will be necessary to study a large ensemble of different proteins. Such a study is justified in the context of specific problems like monitoring the consequences of mutation on protein surface accessibility and on intraprotein compactness.

ACKNOWLEDGMENTS

This work was supported by the Italian Government, Fondi 40% 1995, and by Human Capital (EC), Contract ERBCHRXCT930112. K. B., M. L., and J. R. acknowledge financial support obtained by the Belgian FNRS as a contribution to the LEA (CNRS-FNRS).

REFERENCES

1. E. Locci, K. Bartik, M. Luhmer, M. Casu, G. Saba, A. Lai, and J. Reisse, Probing hydrophobic cavities in myoglobin by ^{129}Xe NMR spectroscopy, *in* Keystone Symposia, "Frontiers of NMR in Molecular Biology VI," January 9–15, 1999, Breckenridge, CO, p. 53, Abstract E216.
2. E. Locci, K. Bartik, M. Luhmer, M. Casu, G. Saba, A. Lai, and J. Reisse, Probing protein cavities and surfaces by ^{129}Xe NMR spectroscopy, *in* Xe-MAT 2000, "Optical Polarization and Xenon NMR of Materials," June 28–30, 2000, Sestri Levante, Italy, p. 46. (Abstract)
3. C. J. Jameson, "Multinuclear NMR," pp. 1–463, Plenum Press, New York, 1987.
4. J. Reisse, Monoatomic xenon: Its great interest in chemistry as a probe of intermolecular interactions, and its (easy) study by NMR, *N. J. Chem.* **10,** 665–672 (1986).
5. C. Dybowski, N. Bansal, and T. M. Duncan, NMR spectroscopy of xenon in confined spaces: Clathrates, intercalates, and zeolites, *Annu. Rev. Phys. Chem.* **42,** 433–464 (1991).
6. D. Raftery and B. F. Chmelka. Xenon NMR spectroscopy, *in* "NMR Basic Principles and Progress" (B. Blümich, Ed.), pp. 111–157, Springer-Verlag, Berlin, 1994.

7. M. Luhmer, A. Dejaegere, and J. Reisse, Interpretation of the solvent effect on the screening constant of Xe-129, *Magn. Reson. Chem.* **27,** 950–952 (1989).
8. A. Dejaegere, M. Luhmer, M.-L. Stien, and J. Reisse, Study of NMR relaxation of xenon-131 in quadrupolar solvents, *J. Magn. Reson.* **91,** 362–374 (1991).
9. A. Moschos and J. Reisse, Nuclear magnetic relaxation of xenon-129 dissolved in organic solvents, *J. Magn. Reson.* **95,** 603–606 (1991).
10. M. Luhmer, D. Van Belle, J. Reisse, M. Odelius, J. Kowalewski, and J. Laaksonen, Magnatic relaxation of xenon-131 dissolved in benzene. A study by molecular dynamics and Monte Carlo simulations, *J. Chem. Phys.* **98,** 1566–1578 (1993).
11. M. Luhmer and J. Reisse, Molecular dynamics simulation study of the NMR relaxation of xenon-131 dissolved in 1,3-dioxane and in 1,4-dioxane, *J. Magn. Reson. A* **115,** 197–205 (1995).
12. M. Luhmer and K. Bartik, Group contribution analysis of xenon NMR solvent shifts, *J. Phys. Chem.* **101,** 5278–5283 (1997).
13. M. Luhmer and J. Reisse, Quadrupole NMR relaxation of the noble gases dissolved in simple liquids and solutions: A critical review of experimental data in the light of computer simulation results, *Prog. Nucl. Magn. Reson. Spectrosc.* **33,** 57–76 (1998).
14. M. Luhmer, A. Moschos, and J. Reisse, Intermolecular dipole–dipole spin relaxation of xenon-129 dissolved in benzene. A molecular-dynamics simulation study, *J. Magn. Reson. A* **113,** 164–168 (1995).
15. M. Claessens, O. Fabre, D. Zimmermann, and J. Reisse, NMR study of molecular interactions between xenon and crown ethers, *Bull. Soc. Chim. Belg.* **93,** 983–989 (1984).
16. K. Bartik, M. Luhmer, S. J. Heyes, R. Ottinger, and J. Reisse, Probing molecular cavities in α-cyclodextrin solutions by xenon NMR, *J. Magn. Reson. B* **109,** 164–168 (1995).
17. K. Bartik, M. Luhmer, J. P. Dutasta, A. Collet, and J. Reisse, ^{129}Xe and ^{1}H NMR study of the reversible trapping of xenon by cryptophane-A in organic solution, *J. Am. Chem. Soc.* **120,** 784–791 (1998).
18. M. Luhmer, B. M. Goodson, Y.-Q. Song, D. D. Laws, L. Kaiser, M. C. Cyrier, and A. Pines, Study of xenon binding in cryptophane-A usng laser-induced NMR polarization enhancement, *J. Am. Chem. Soc.* **121,** 3502–3512 (1999).
19. K. Bartik, M. El Haouaj, M. Luhmer, A. Collet, and J. Reisse, Can monoatomic xenon become chiral? *Chem. Phys. Chem.* **1,** 221–224 (2000).
20. K. Bartik, M. Luhmer, A. Collet, and J. Reisse, Molecular polarization and molecular chiralization: The first example of a chiralized xenon atom, *Chirality* **13,** 2–6 (2001).
21. G. Saba, M. Casu, and A. Lai, Application of quadrupolar ^{131}Xe-NMR relaxation to the study of macromolecular systems, *Int. J. Quantum Chem.* **59,** 343–348 (1996).
22. A. A. Rashin, M. Iofin, and B. Honig, Internal cavities and buried waters in globular proteins, *Biochemistry* **25,** 3619–3625 (1986).
23. S. J. Hubbard, K. H. Gross, and P. Argos, Intramolecular cavities in globular proteins, *Protein Eng.* **7,** 613–626 (1994).
24. M. A. Williams, J. M. Goodfellow, and J. M. Thornton, Buried waters and internal cavities in monomeric proteins, *Protein Sci.* **3,** 1224–1235 (1994).
25. S. J. Hubbard and P. Argos, Cavities and packing at protein interfaces, *Protein Sci.* **3,** 2194–2206 (1994).
26. B. P. Schoenborn, H. C. Watson, and J. C. Kendrew, Binding of xenon to sperm whale myoglobin, *Nature* **207,** 28–30 (1965).
27. B. P. Schoenborn and C. L. Nobbs, The binding of xenon to sperm whale deoxymyoglobin, *Mol. Pharmacol.* **2,** 495–498 (1966).
28. B. P. Schoenborn, Structure of alkaline metmyoglobin–xenon complex, *J. Mol. Biol.* **45,** 297–303 (1969).
29. B. P. Schoenborn, Binding of xenon to horse hemoglobin, *Nature* **208,** 760–762 (1965).
30. R. F. Tilton, Jr., I. D. Kuntz, Jr., and G. A. Petsko, Cavities in proteins: Structure of a metmyoglobin–xenon complex solved to 1.9 Å, *Biochemistry* **23,** 2849–2857 (1984).
31. G. J. Ewing and S. Maestas, The thermodynamics of absorption of xenon by myoglobin, *J. Phys. Chem.* **74,** 2341–2344 (1970).
32. R. F. Tilton, Jr., and I. D. Kuntz, Jr., Nuclear magnetic resonance studies of xenon 129 with myoglobin and hemoglobin, *Biochemistry* **21,** 6850–6857 (1982).
33. M. Schiltz, T. Prangé, and R. Fourme, On the preparation and X-ray data collection of isomorphous xenon derivatives, *J. Appl. Cryst.* **27,** 950–960 (1994).
34. M. Schiltz, R. Fourme, I. Broutin, and T. Prangé, The catalytic site of serine proteinases as a specific binding cavity for xenon, *Structure* **3,** 309–316 (1995).
35. T. Prangé, M. Schiltz, L. Pernot, N. Colloc'h, S. Longhi, W. Bourguet, and R. Fourme, Exploring hydrophobic sites in proteins with xenon or krypton, *Proteins* **30,** 61–73 (1998).
36. R. F. Tilton, Jr., U. C. Singh, I. D. Kuntz, Jr., and P. A. Kollmann, Protein–ligand dynamics. A 96 picosecond simulation of a myoglobin–xenon complex, *J. Mol. Biol.* **199,** 195–211 (1988).
37. R. F. Tilton, Jr., U. C. Singh, S. J. Weiner, M. L. Connlly, I. D. Kuntz, Jr., and P. A. Kollmann, Computational studies of the interaction of myoglobin and xenon, *J. Mol. Biol.* **192,** 443–456 (1986).
38. C. R. Bowers, V. Storhaug, C. E. Webster, J. Bharatam, A. Cottone III, R. Gianna, K. Betsey, and B. J. Gaffney, Exploring surfaces and cavities in lipoxygenase and other proteins by hyperpolarized xenon-129 NMR, *J. Am. Chem. Soc.* **121,** 9370–9377 (1999).
39. A. Stith, T. K. Hitchens, D. P. Hinton, S. S. Berr, B. Driehuys, J. R. Brookeman, and R. G. Bryant, Consequences of ^{129}Xe–^{1}H cross relaxation in aqueous solutions, *J. Magn. Reson.* **139,** 225–231 (1999).
40. S. M. Rubin, M. M. Spence, B. M. Goodson, D. E. Wemmer, and A. Pines, Evidence of nonspecific surface interactions between laser-polarized xenon and myoglobin in solution, *Proc. Natl. Acad. Sci. USA* **97,** 9472–9475 (2000).
41. E. Breslow, Changes in side chain reactivity accompanying the binding of heme to sperm whale apomyoglobin, *J. Biol. Chem.* **239,** 486–496 (1964).
42. T. Imoto and J. A. Rupley, Oxidation of lysozyme by iodine: Identification and properties of an oxindolyl ester intermediate: Evidence for participation of glutamic acid 35 in catalysis, *J. Mol. Biol.* **80,** 657–667 (1973).
43. D. W. Smith and J. P. Williams, Analysis of the visible spectra of some sperm-whale ferrimyoglobin derivatives, *Biochem. J.* **110,** 297–301 (1968).
44. Y. Yamamoto, A. Osawa, Y. Inoue, R. Chujo, and T. Suzuki, A ^{1}H-NMR study of electronic structure of the active site of *Galeorhinus Japonicus* metmyoglobin, *Eur. J. Biochem.* **192,** 225–229 (1990).
45. P. Alard, "Calculs de Surface et d'Énergie dans le Domaine des Macromolécules," Ph.D. thesis, Université Libre de Bruxelles, 1991.
46. R. H. Kretsinger, H. C. Watson, and J. C. Kendrew, Binding of mercury–iodide and related ions to crystals of sperm whale metmyoglobin, *J. Mol. Biol.* **31,** 305–314 (1968).
47. W. H. Press, B. P. Flannery, S. A. Teukolsky, and W. T. Vetterling, "Numerical Recipes in C," Cambridge Univ. Press, Cambridge, 1998.